Check for updates

Advances in Materials Science and Engineering

WILEY

RESEARCH ARTICLE OPEN ACCESS

A Smart Window Based on Reversible Metal Electrodeposition (RME) With Tin and Copper

Rebecca Cizek[1,2] | Stephan J. Heise[1] | Florian Sutter[3] | Peter Heller[3] | Robert Pitz-Paal[2,4]

[1]Institute of Solar Research, Deutsches Zentrum für Luft- und Raumfahrt (German Aerospace Center DLR), Oldenburg, Germany | [2]Faculty of Mechanical Engineering, RWTH Aachen University, Aachen, Germany | [3]Institute of Solar Research, Deutsches Zentrum für Luft- und Raumfahrt (German Aerospace Center DLR), Almeria, Spain | [4]Institute of Solar Research, Deutsches Zentrum für Luft- und Raumfahrt (German Aerospace Center DLR), Cologne, Germany

Correspondence: Rebecca Cizek (rebecca.cizek@dlr.de)

Received: 12 November 2025 | **Revised:** 15 June 2026 | **Accepted:** 25 June 2026

Academic Editor: Mohammad Rezwan Habib

Keywords: dynamic window | self-bleaching | smart window | switchable window | time-resolved transmittance

ABSTRACT

The optical transmittance of smart windows can be modulated on demand, rendering them suitable for use in building facades, automobile mirrors, windows, display screens, and greenhouses. This study investigates reversible metal electrodeposition (RME) smart windows using a nontoxic, solid-like electrolyte based on tin and copper. Among the various switching methods, RME has been demonstrated to be cost-effective, scalable, and color-neutral. Solid-like electrolytes maintain electrode spacing over time and minimize leakage risks; however, they are typically composed of toxic substances. In this study, we present a nontoxic, solid-like electrolyte that exhibits a coulombic efficiency (CE) of 45.7%. To elucidate the alterations in transmittance, time-resolved measurements were conducted during the coloration and bleaching processes. The coloration rate was found to range from 39% to 55% per minute at a potential of −1.5 V compared to an indium tin oxide (ITO) electrode, applied for a duration of 60 s. The transmittance was measured from the ultraviolet (UV) to the near infrared (NIR) spectral range in both the initial state and the colored states. The average visual transmittance (AVT) between 380 and 750 nm ranges from 80.8% to 14.2%, with chroma ranging from 1 to 11, indicating color neutrality. Cyclic voltammetry measurements were conducted on a finished smart window to analyze the chemical reactions occurring during the coloration and bleaching processes. Further, the present study compares the self-bleaching mechanism (bleaching without applied voltage) of the RME window to recent studies in the field. Finally, the study also addresses reversibility and cycling stability deficiencies.

1 | Introduction

A substantial proportion of global energy consumption is attributable to buildings, accounting for approximately 40% of the total consumption [1]. Smart windows have been demonstrated to effectively mitigate energy consumption for heating and cooling by modulating the influx of light and heat into the interior of a building [2, 3]. A comparison of smart windows integrated into buildings with static shading solutions has shown that the former can further reduce energy consumption by 10%–20% due to their adaptability to weather and seasonal changes [2, 3]. Moreover, the integration of smart windows into architectural design has been demonstrated to enhance occupant well-being and productivity, thereby contributing to an improvement in the quality of life. [4–6]. The optical transmittance of smart windows can be modulated on demand in response to an optical, electrical, or mechanical stimulus. The methods employed to modify the optical transmittance of such windows

This is an open access article under the terms of the Creative Commons Attribution License, which permits use, distribution and reproduction in any medium, provided the original work is properly cited.

Copyright © 2026 Rebecca Cizek et al. *Advances in Materials Science and Engineering* published by John Wiley & Sons Ltd.

can be classified as photochromic, thermochromic, mechanochromic, or electrochromic [7, 8]. Smart windows, which are already available on the market, are being integrated into buildings by companies such as Saint-Gobain, Gauzy, Miru Smart Technologies, and numerous others. Grand View Research, Inc. forecasts that the market will expand from 7.38 billion USD in 2024 to 13.01 billion USD by 2030 [9]. Reversible metal electrodeposition (RME)-based smart windows benefit from low-cost and solution-processable fabrication methods. This alternative offers a more scalable approach in comparison to vacuum-based techniques [10], including tungsten trioxide (WO_3) [11, 12]. RME windows modulate light transmittance through the reversible electrodeposition of metals. The application of a cathodic (negative) potential leads to the reduction of metal ions (Mn^+) within the electrolyte, thereby forming a metallic layer on one electrode. Concurrently, a counter-anion (R) undergoes oxidation to form an oxide (O), as depicted in Equations (1) and (2)

$$M^{n+} + ne^- \rightleftharpoons M \quad (1)$$

$$R \rightleftharpoons O^{n+} + ne^- \quad (2)$$

The reversal of polarity results in the dissolution of the deposited metal, thereby restoring the specimen's transparency. The existing body of literature thoroughly documents the phenomenon of redox-based switching [13–23]. A salient feature of RME windows is self-bleaching, a process in which the colored state undergoes a transition due to the dissolution of the metal into the electrolyte, obviating the necessity for external power sources. The period preceding the onset of self-bleaching is designated as resting stability [24]. Self-bleaching is associated with the chemical stability of the deposited metal layer that is responsible for the coloration of the window. A substance is said to be chemically stable when it exhibits a retention of its chemical composition and properties over an extended period, exhibiting minimal alteration. In the case of a smart window with an electrolyte, chemical stability is demonstrated by the system's ability to return to the initial state after a change in transmittance. The system demonstrates optimal cycling stability when the coloration and bleaching processes can be replicated multiple times, and the initial state is restored following each switching cycle (i.e., coloration and bleaching). The solid-like electrolyte produced in this study combines the benefits of both liquid and solid electrolytes. This approach has been demonstrated to enhance operational safety, as outlined in reference [25]. Liquid electrolytes are susceptible to leakage, the formation of bubbles due to gas evolution during operation, and exhibit limited chemical stability [26, 27]. While solid electrolytes enhance stability and mitigate leakage risks [28], they are characterized by low ionic conductivity and inadequate interfacial contact [26, 27]. Conventional electrochromic devices frequently utilize heavy metals or hazardous materials. The system presented in this study utilizes nontoxic components, including copper (Cu), tin (Sn), lithium perchlorate ($LiClO_4$), water (H_2O), and dimethyl sulfoxide (DMSO), ensuring its safety for use in consumer and agricultural environments. The present study builds upon the system studied by Eh et al. [25], who used Cu and Sn in a solid-like electrolyte with lithium bis(trifluoromethanesulfonyl) imide (LiTFSI) and potassium iodide (KI) and demonstrated the effectiveness of a tristate device. In contrast, we use lithium perchlorate ($LiClO_4$), omitted KI, and add water (H_2O), which enhances the bleaching process. This smart window features a unique electrolyte combination of tin(II) chloride ($SnCl_2$), copper(II) chloride ($CuCl_2$), lithium perchlorate ($LiClO_4$), deionized water, DMSO, and polyvinyl acetate (PVA).

Each ingredient is carefully chosen for its good switchability and optimized self-bleaching properties. The combination of Sn and Cu increases cycle stability, shortens coloration time, and minimizes surface oxidation of the deposited layer [25, 29]. Unlike nickel, copper and tin are relatively inexpensive and nontoxic. [30]. When combined with chlorine ions (Cl^-), copper (Cu) can improve the homogeneity of the deposited metal layer [29]. The presence of Cl^- ions in the electrolyte promotes the formation of copper chloride (CuCl) and improves the efficiency of metal electrodeposition and dissolution [16, 31]. Lithium improves ionic conductivity, leading to increased switching speed [25, 26, 32]. The standard potential of Cu/Cu^{2+} is positive [15, 33], indicating good attributes for RME windows. DMSO is used as a solvent and has a wide voltage range of −3.45 to 0.95 V versus Ag/Ag^+ [34]. Water improves the solubility of metal salts, and its polarity helps deposit metals [35]. PVA acts as a thickener, helping to create a semisolid electrolyte for easier handling. The electrolyte is placed in a sealing ring between two indium tin oxide (ITO) electrodes, as depicted in Figure 1.

In this paper, we investigate whether a solid-like, nontoxic electrolyte based on RME with Cu and Sn can be used for a smart window application with optimized self-bleaching ability. To this end, we conduct an investigation into the general switching abilities, including coloration and bleaching processes, and compare the results with data from other sources. This investigation includes transmittance measurements between 200 and 2500 nm for different states of the samples, as well as time-resolved transmittance measurements during the coloration and bleaching processes and cyclic voltammetry measurements.

2 | Results

We demonstrated the functionality of the smart window device by investigating the coloration, bleaching, and self-bleaching processes. First, we evaluated the chemical reactions during coloration and bleaching by analyzing cyclic voltammetry measurements. Then, we demonstrated a complete switching cycle consisting of coloration and bleaching in a time-resolved measurement. Next, we examined the self-bleaching properties before analyzing the transmittance spectra.

Before applying a voltage, the salts in the electrolyte dissociate:

$$CuCl_2 \longrightarrow Cu^{2+} + 2Cl^- \quad (3)$$

$$SnCl_2 \longrightarrow Sn^{2+} + 2Cl^- \quad (4)$$

$$LiClO_4 \longrightarrow Li^+ + ClO_4^- \quad (5)$$

In chlorine-rich environments, Sn^{2+} and Cu^{2+} ions may form complexes, for example: $Cu^{2+} + 4Cl^- \rightleftharpoons [CuCl_4]^{2-}$ and $Sn^{2+} + 3Cl^- \rightleftharpoons [SnCl_3]^-$. Lithium (Li) and ClO_4^- ions act as ionic conductors. It can be assumed that the presence of tin and copper is indicative of their deposition on the anode, given that no other factor could account for the observed change in transmittance. However, it should be noted that this hypothesis was not

5928, 2026, 1, Downloaded from https://onlinelibrary.wiley.com/doi/10.1155/amse/9976638 by Dtsch Zentrum F. Luft-U. Raum Fahrt in D. Helmholtz Gemein., Wiley Online Library on [22/09/2026]. See the Terms and Conditions (https://onlinelibrary.wiley.com/terms-and-conditions) on Wiley Online Library for rules of use; OA articles are governed by the applicable Creative Commons License

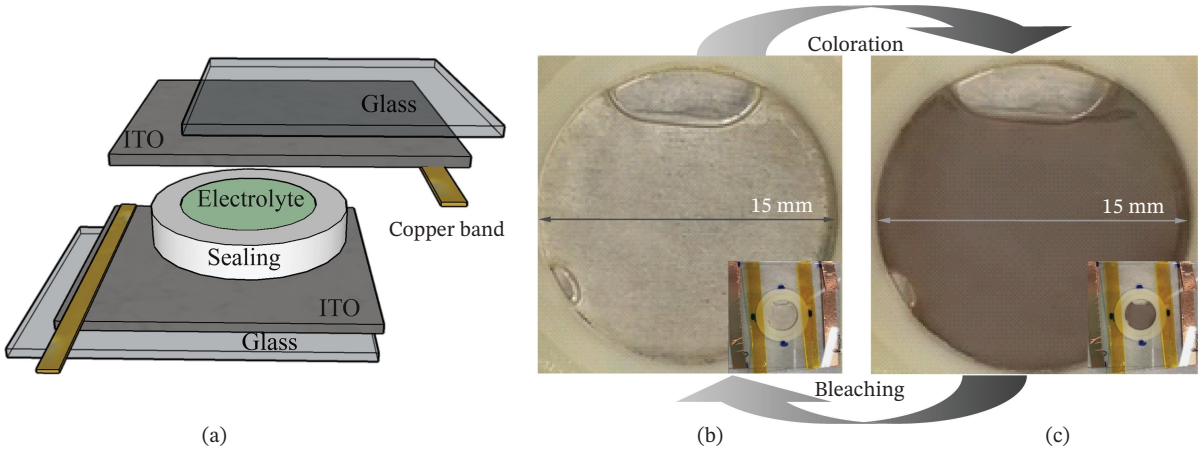


FIGURE 1 | (a) Schematic representation of the configuration of the two-electrode smart window produced in the present study (not to scale). The electrolyte is positioned between two glass slides covered with indium tin oxide (ITO). The glass has a thickness of 1.1 mm, the ITO layer is 60 nm thick, and the electrolyte is 0.5 mm thick. The device is contacted through self-adhesive copper bands, which are in contact solely with the ITO and not with the electrolyte due to a sealing mechanism. (b) Illustration of the transparent window state of the active area with an inlay of the entire device, positioned horizontally on a white surface. (c) Illustration of the colored window state of the active area with an inlay of the whole device. The images were captured from a video documenting the coloration process of Window A (see Supporting Information, Video 1), which had an active area with a diameter of 15 mm. The air bubble will be discussed in greater detail in Section 3.

supported by scanning electron microscope (SEM) measurements. The process of bleaching theoretically results in the oxidation and subsequent dissolution of the deposited metals into the electrolyte. The described reactions are likely to be the fundamental cause of the alteration in transmittance. Figure 2 shows a cyclic voltammetry measurement conducted on Window D, where the peaks are related to the chemical reactions that occur during the coloration and bleaching processes.

The cathodic peak at an internal potential of approximately $-0.3\,\mathrm{V}$ (I_c) is associated with the reduction of copper, $Cu^{2+} + e^- \longrightarrow Cu^+$. The cathodic peak at $-0.8\,\mathrm{V}$ (II_c) is indicative of the reduction of tin, $Sn^{2+} + 2e^- \longrightarrow Sn$. It appears that the complete reduction of copper occurs at a voltage of $-1.05\,\mathrm{V}$ (III_c). This reaction is represented by the following equation: $Cu^+ + e^- \longrightarrow Cu$. That leads to the assumption that first tin is deposited on the cathode and then copper. The reversal of the voltage application leads to the oxidation of Cu^+ to Cu^{2+} at an applied potential of $0.05\,\mathrm{V}$ (I_a): $Cu^+ \longrightarrow Cu^{2+} + e^-$. The visual impression suggests that the tin has undergone oxidation, transforming from Sn to Sn^{2+}. However, this transformation is not reflected in the measurement, which does not show any peaks indicative of such a transition. The subsequent discussion will address the peaks and their position in more detail and compare the results to other publications to determine their significance. Although cyclic voltammetry furnishes information regarding metals and metal salts, the counterreaction remains ambiguous. This subject will be addressed subsequently.

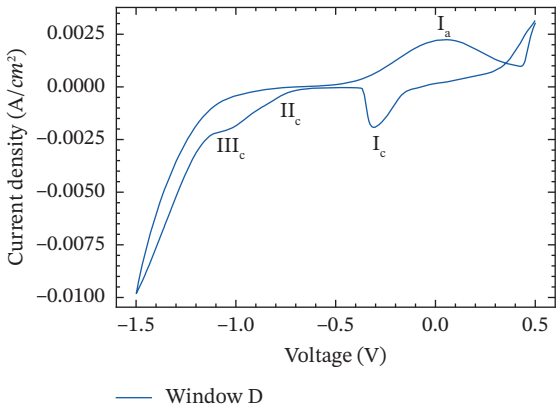


FIGURE 2 | A cyclic voltammetry measurement was conducted on Window D, ranging from 0.5 to $-1.5\,\mathrm{V}$, with a scan rate of 10 mV/s. The cathodic peaks are observed at $I_c \approx -0.3\mathrm{V}$, $II_c \approx -0.8\mathrm{V}$, $III_c \approx -1.05\mathrm{V}$, and an anodic peak at $I_a \approx 0.05\mathrm{V}$.

In the application, smart windows are utilized by means of an electrical voltage that is applied for a designated period of time. This results in a modification of the transmittance of the system. Utilizing an opposing voltage results in the bleaching of the smart window. As illustrated in Figure 1(b,c), Window A is depicted in both its colored and bleached states. The application of a voltage of $-1.5\,\mathrm{V}$ versus ITO for a duration of 60 s resulted in the coloration of the window. For the bleaching process, a voltage of $0.3\,\mathrm{V}$ versus ITO was employed for the same duration. Videos illustrating the coloration (Video 1) and bleaching (Video 2) processes are available in the supporting information. The parameters were found to demonstrate adequate switchability without causing damage to the device. Higher voltages frequently result in incomplete bleaching and damaged the device.

The switching between the colored and bleached states of Window A was repeatable, but in other samples, it was more difficult to achieve the same repeatability. The same switching parameters and the same sample (Window A) were used for the measurements in Figure 3(a). In this instance, the red data illustrate the time-resolved switching process as previously described. As the coloration processed, there was a notable shift in transmittance, with a decrease from approximately 65% to 10%, corresponding to a coloration rate of 55% per minute. Subsequently, the window underwent a bleaching process, resulting in a consistent escalation in transmittance at a rate of 45% per minute. When the voltage application was terminated at the two-

5928, 2026, 1, Downloaded from https://onlinelibrary.wiley.com/doi/10.1155/amse/9976638 by Dtsch Zentrum F. Luft-U. Raum Fahrt in D. Helmholtz Gemein., Wiley Online Library on [22/09/2026]. See the Terms and Conditions (https://onlinelibrary.wiley.com/terms-and-conditions) on Wiley Online Library for rules of use; OA articles are governed by the applicable Creative Commons License

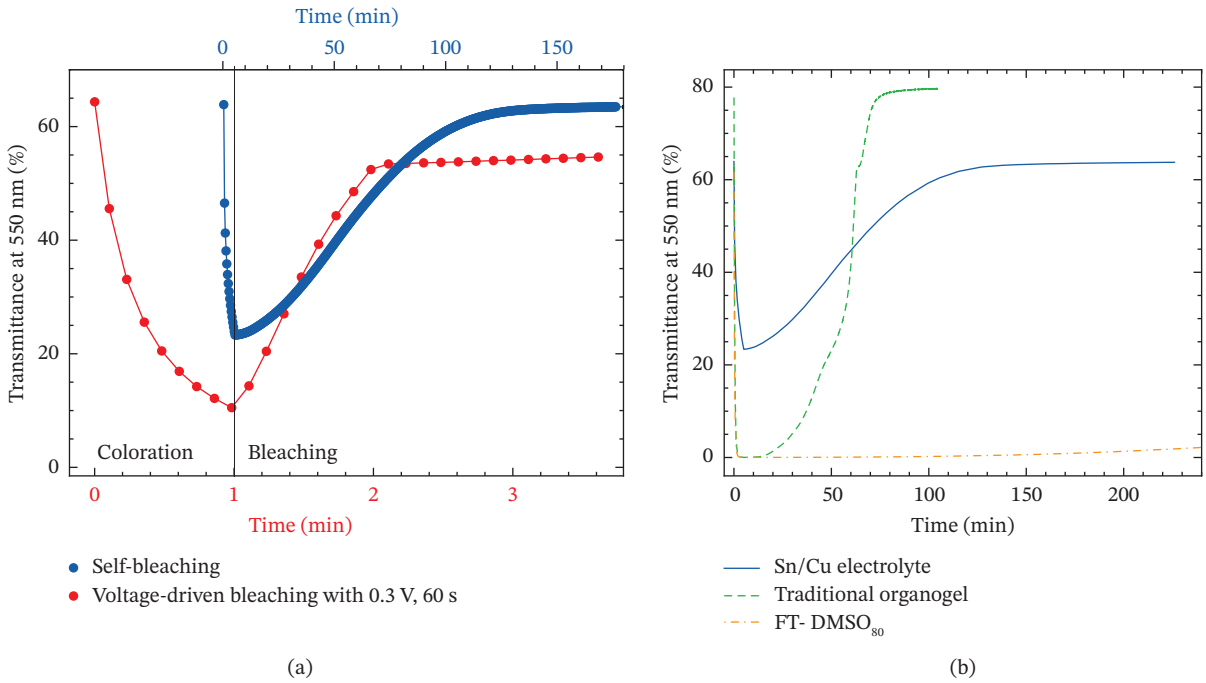


FIGURE 3 | (a) Transmittance at 550 nm during bleaching and self-bleaching as a function of time. The graphs show the coloration and bleaching process to compare the voltage-driven bleaching and the self-bleaching, as well as the coloration process. For better comparison of the bleaching processes, the point where the bleaching starts is aligned for both measurements. Smart Window A was colored at −1.5 V versus ITO for 5 min before the voltage application was stopped (blue). The same window was then colored with −1.5 V versus ITO for 60 s and bleached with 0.3 V versus ITO for 60 s (red). The self-bleaching reaches the initial transmittance of the measurement after 147 min. (b) Comparison of the self-bleaching with different electrolytes. The blue line is equal to the blue measurement in (a). All samples in (b) are colored for 5 min. The green and yellow dash-dotted lines are colored with −3 V versus Ag/Ag^+ and show data from Guo et al. [36] with their approval. The smart Window A was colored with only −1.5 V versus ITO (blue, solid). After the coloration, no voltage was applied to any of the three samples while the measurement of the transmittance was ongoing.

minute mark, a transmittance of approximately 55% was attained. This finding suggests that, in principle, the transmittance of the smart window can be modulated by applying voltages in both directions. The coulombic efficiency (CE) was determined through the calculation of the measured current during the processes of coloration and bleaching. The CE is expressed as $CE\ (\%) = Q_{Strip}/Q_{deposit} \times 100$. The quantity Q denotes the current density in relation to the active area of the smart window. The initial analysis indicated that Window A exhibited the optimal reversibility compared to the other samples, yet its CE remained at 45.7%.

These observations strongly suggest the presence of side reactions and compromised cycle stability. The following windows demonstrate a satisfactory degree of self-bleaching capability, which is commensurate with a minimal degree of resting stability. It has been demonstrated that both self-bleaching and resting stability are related to the chemical stability of the device. As illustrated in Figure 3(b), a clear distinction emerges between the samples of this study and those that have been optimized for enhanced resting stability. The yellow dash-dotted line indicates a window that exhibits optimal long-term stability in its colored state. The green dashed line illustrates a sample with organogel [36] and has self-bleaching properties similar to those of the sample of this study (blue solid line). The concept of promoting self-bleaching entails the integration of the aforementioned practice as a component of a broader system, thereby facilitating the development of a self-regulating apparatus, particularly in the context of greenhouse applications. The duration of the self-bleaching process can be modified to coincide with the periods of sunlight during the day. Another application example is the direct contact with a transparent PV on only one side. In this scenario, the PV and the smart window share a single electrode. It must be acknowledged that this has not been thoroughly tested, and further research is required in this field. The blue data in Figure 3 demonstrate the coloration and self-bleaching process in a time-resolved measurement. In this instance, the coloration process was executed at a voltage of −1.5 V compared to the ITO, with a duration of 5 min. This resulted in a coloration rate of 8.5% per minute. As demonstrated in Figure 3(a), the blue line attained the initial value of the measurement after approximately 145 min, as indicated by the blue time line situated at the top of the diagram. The underlying mechanisms responsible for the self-bleaching phenomenon and the concomitant dissolution of the metal layer remain to be elucidated. It has been demonstrated that this window can be bleached through the implementation of self-bleaching techniques, as opposed to the conventional method of applying a voltage. This results in prolonged bleaching times, with a bleaching rate of 0.28% per minute in comparison to 45% per minute in the case of voltage-powered bleaching. These switching properties must be taken into consideration when designing an application.

The transmittance spectra over a wavelength range from 200 to 2500 nm demonstrate the capacity for light modulation in smart windows (see Figure 4). As illustrated in Figure 4(b), the blue and green lines correspond to the same sample and demonstrate the variation in transmittance prior to and following the initial

5928, 2026, 1, Downloaded from https://onlinelibrary.wiley.com/doi/10.1155/amse/9976638 by Dtsch Zentrum F. Luft-U. Raum Fahrt in D. Helmholtz Gemein., Wiley Online Library on [22/09/2026]. See the Terms and Conditions (https://onlinelibrary.wiley.com/terms-and-conditions) on Wiley Online Library for rules of use; OA articles are governed by the applicable Creative Commons License

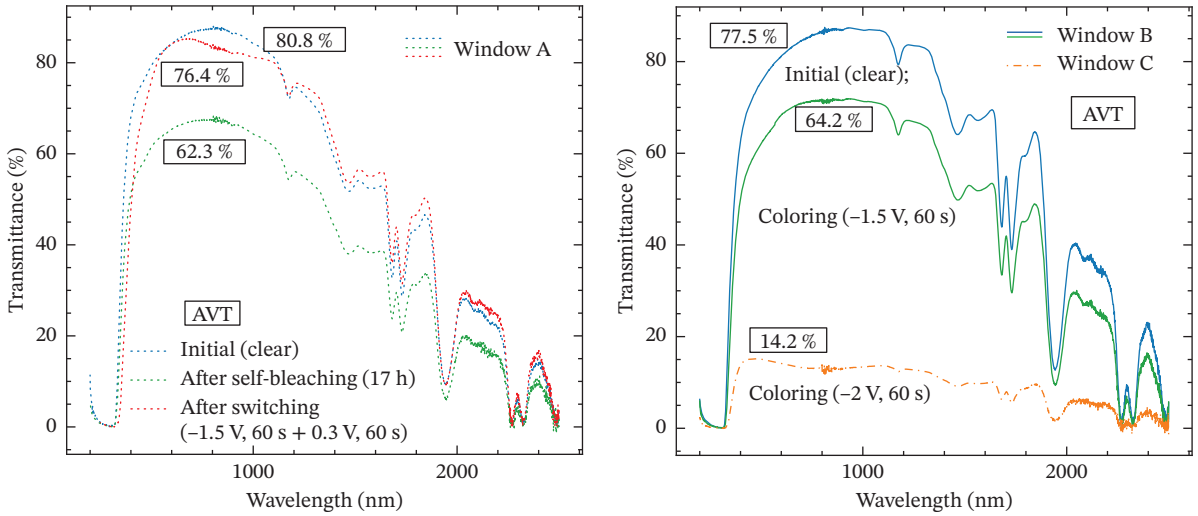


FIGURE 4 | Transmittance spectra of different smart windows (A, B, and C) in different states (initial, colored, bleached, and switched). (a) Window A in the initial, self-bleached, and switched states. (b) Window B in the initial state and colored with −1.5 V versus ITO for 60 s, and Window C in the colored state with −2 V versus ITO for 60 s. The related AVT is presented in a box next to the graph.

coloration procedure at −1.5 V versus ITO for 60 s. Window C was subjected to coloration at −2 V versus ITO for 60 s, resulting in a diminished transmittance. The initial transmittance exhibited a notable similarity to the blue line of Window B. The overall transmittance of the windows depicted in Figure 4 has been quantified using the average visual transmittance (AVT) displayed in boxes within the diagram. The experimental results demonstrated a range of transmittance values from 80.8% to 14.2% within the AVT range. This suggests a considerable range of transmittance that can be adjusted as required. The transmittance depends on the applied voltage and the duration of voltage application. Within the visual range, the transmittance remains relatively constant, thereby indicating a neutral color appearance. The chroma values were calculated from UV–Vis–NIR data (Figure 4(a)), as described in [37] and summarized in Table 1. The CIELAB [37] coordinates a^* and b^* were computed using the program CODE.

As illustrated in Figure 4(a), Window A demonstrates the feasibility of achieving the initial state subsequent to multiple switching cycles, as indicated by the red dotted line. This finding suggests that the window is capable of dissolving the majority of the deposited metal layer; however, this phenomenon does not occur in every instance of bleaching and only for Window A. Furthermore, Figure 3(a) demonstrates the self-bleaching measurement, indicated by the blue trace, which reverts to its initial state. This observation signifies the potential stability of the electrolyte and the potential for good reversibility, although it was an exception in this study. The precise sequence of measurements is delineated in Table 2. This finding suggests that Window A exhibits sufficient dissolution capacity for the majority of the deposited metal layer. This suggests that the window may also exhibit adequate cycle stability, which could in turn indicate satisfactory lifetime stability. However, it should be noted that achieving this level of stability is not guaranteed in every instance. A multitude of issues have been identified as contributing to suboptimal reproducibility. It was observed that only one sample demonstrated adequate reproducibility prior to the onset of degradation. Approximately 6 months following the manufacturing of the smart windows, they deteriorated to the point that they are no longer functional, and the color changed to a more yellowish stain.

TABLE 1 | Chroma values of the spectra shown in Figure 4.

Chroma values	
Window A: Initial (clear) state	5.34
Window A: After self-bleaching (17 h)	5.62
Window A: After switching (−1.5 V for 60 seconds + 0.3 V for 60 seconds)	11.05
Window B: Initial (clear) state	5.99
Window B: After coloration (−1.5 V for 60 seconds)	6.75
Window C: After coloration (−2 V for 60 seconds)	1.68

3 | Discussion

This study demonstrates that smart windows have the capacity to modulate light transmittance in a color-neutral manner using a nontoxic, solid-like electrolyte. These findings are consistent with previous reports on RME [16, 17, 25, 36, 38, 39].

Cyclic voltammetry analysis of the coloration and bleaching process (see Figure 2) shows results comparable to those in [25]. When comparing the peak positions, the similarities become clearer, as shown in the following. Eh et al. observed a cathodic peak at −0.36 V during the reduction of Cu^{2+} to Cu^{+}. This agrees

5928, 2026, 1, Downloaded from https://onlinelibrary.wiley.com/doi/10.1155/amse/9876638 by Dtsch Zentrum F. Luft-U. Raum Fahrt in D. Helmholtz Gemein., Wiley Online Library on [22/09/2026]. See the Terms and Conditions (https://onlinelibrary.wiley.com/terms-and-conditions) on Wiley Online Library for rules of use; OA articles are governed by the applicable Creative Commons License

TABLE 2 | Measurement sequence Window A.

Date	Type of measurement	Parameters	Figure, color, line style
05.12.24	Glass washing		
05.12.24	Deposition of 60 nm ITO		
06.12.24	Production of electrolyte		
06.12.24	Window assembly		
12.12.24	Transmittance	200–2500 nm	Figure 3(a) blue dotted line
12.12.24	Cyclic voltammetry transmittance	0.2 to −1.5 V, 0.05 V/s, 700 cycles 540–560 nm	
13.12.24	Transmittance	200–2500 nm	
14.12.24	Transmittance	200–2500 nm	
14.12.24	Constant voltage, video	−1.5 V, 60 s	Figure 1(b,c)
14.12.24	Constant voltage, video	0.3 V, 60 s	
14.12.24	Constant voltage	−1.5 V, 60 s, 0.3 V, 60 s	
14.12.24	Constant voltage, video	−1.5 V, 60 s, 0.3 V, 60 s	
16.12.24	Transmittance	200–2500 nm	Figure 3(a) green dotted line
16.12.24	Constant voltage + open circuit voltage (OCV) + transmittance	−1.5 V, 5 min OCV for 220 min 540–560 nm	Figure 2(a) blue line, Figure 2(b) blue line, Figure 4 blue line
16.12.24	Transmittance	200–2500 nm	
16.12.24	Constant voltage, video	−1.5 V, 60 s	
16.12.24	Constant voltage, video	0.3 V, 60 s	
17.12.24	Transmittance	200–2500 nm	
17.12.24	Cyclic voltammetry + transmittance	0.2 to −1.5 V, 0.05 V/s, 20 cycles 540–560 nm	
17.12.24	Transmittance	200–2500 nm	
17.12.24	Constant voltage	0.3 V, 60 s	
17.12.24	Constant voltage	−1.5 V, 60 s	
04.02.25	Constant voltage	−1.5 V, 60 s	
04.02.25	Constant voltage	0.3 V, 60 s	
04.02.25	Constant voltage	0.3 V, 60 s	
04.02.25	Transmittance	200–2500 nm	
04.02.25	Constant voltage + transmittance	−1.5 V, 60 s 540–560 nm	Figure 4 green line
04.02.25	Transmittance	200–2500 nm	
04.02.25	Constant voltage	0.3 V, 60 s	
06.02.25	Transmittance	200–2500 nm	
06.02.25	Transmittance	200–2500 nm	
06.02.25	Constant voltage + transmittance	−1.5 V, 60 s, 0.3 V, 60 s 560–540 nm	Figure 2(a) red line
06.02.25	Transmittance	200–2500 nm	Figure 3(a) red dotted line
06.02.25	Constant voltage + transmittance	−1.5 V, 60 s, 0.3 V, 60 s 540–560 nm	
10.04.25	Transmittance	200–2500 nm	
14.04.25	Constant voltage	−1.5 V, 60 s	

5928, 2026, 1, Downloaded from https://onlinelibrary.wiley.com/doi/10.1155/amse/9876538 by Dtsch Zentrum F. Luft-U. Raum Fahrt In D. Helmholtz Gemein., Wiley Online Library on [22/09/2026]. See the Terms and Conditions (https://onlinelibrary.wiley.com/terms-and-conditions) on Wiley Online Library for rules of use; OA articles are governed by the applicable Creative Commons License

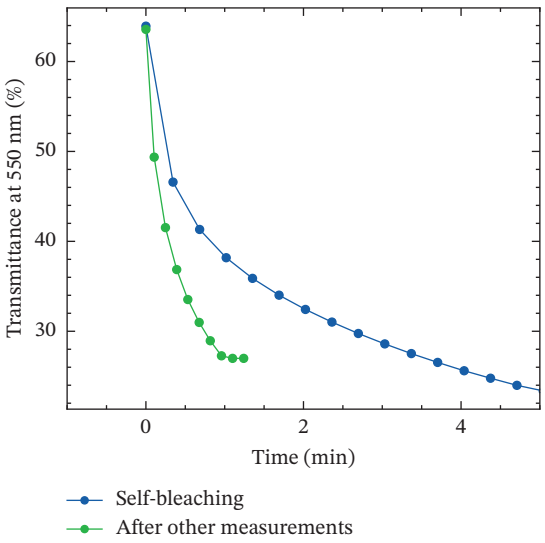


FIGURE 5 | Coloration of Window A at −1.5 V versus ITO in two different measurements. The sample was switched with the same duration of voltage application and the same amount of voltage. The sole discrepancy lies in the time and other measurements conducted between the presented ones. The initial transmittance is nearly equal for both measurements. The earlier measurement (blue, solid line) took longer to fulfill the same change in transmittance than the later measurement (green, solid line), but it could reach lower transmittance values compared to the green, solid line. Table 2 shows the history of the measurements shown here.

well with the findings in this study, which showed a cathodic peak at −0.3 V. The second cathodic peak shown in Eh et al. represents the reduction from Sn^{2+} to Sn. It was found at −0.63 V and shifted toward −0.71 V, indicating an increasing energy barrier to reduce Sn^{2+} electrochemically. In the present study, −0.8 V was measured for the position of the second cathodic peak. Considering the shifting of peaks as well as the fact that the values of this study are conducted versus ITO, we can assume that the peak at −0.8 V is related to the reduction of Sn^{2+} to Sn. The third cathodic peak in [25] was at −0.95 V, which is in good agreement with the −1.05 V found in our study, representing reduction to metallic Cu. The anodic peak at −0.32 V in [25] represents the oxidation of Sn to Sn^{2+} as well as the oxidation of Cu to Cu^{+}. In our study, however, no specific peak was found at that position. Nevertheless, the visible result after bleaching shows that Sn and Cu must be oxidized. According to [25], the second anodic peak, which was found at 0.1 V, is related to the oxidation of Cu^{+} to Cu^{2+}. This aligns with the results of our study. However, one might notice that the peak at 0.05 V is rather wide, which could indicate the presence of multiple peaks, including one for the oxidation of Sn. The difference between our study and that of Eh et al. may also stem from differences in the electrolyte ingredients (see Section 1). This only gives a vague idea of the chemical reactions that might have taken place, but the reduction and oxidation of the metals should always be coupled with a counter reaction on the other electrode. Information about the counter reaction during deposition could not be obtained from measurements, but comparisons to other publications were made. It is most likely that on the anode, a Cl^{-}/ClO^{-} redox reaction takes place, as measured by X-ray photoelectron spectroscopy (XPS) analysis in the study of Guo et al. [38].

A general difference between the present study and other publications occurs due to the setup, which is only a two-electrode system. We did not use a three-electrode system due to the thickness of the electrolyte. It was not possible to fit a third electrode inside without risking contact with one of the two ITO electrodes. Therefore, the measured voltage may differ from that of other studies. We conducted a test measurement with only our electrolyte, ITO electrodes, and a platinum reference electrode, but not with a complete window setup. The electrolyte was in contact with air. The results showed negligible differences between the ITO and platinum within the scope of this study.

The setup also allows for upscaling only by adjusting the sealing. The limiting factor in the scalability is the size of the glass sample that can be covered with ITO. It is to be expected that an increase in size will also cause changes in the thickness of the deposited metal during the coloration throughout the device. This leads to inhomogeneous coloration, which can be reduced by using metal meshes [17, 22].

For the sample size presented here, the color was rather neutral, which can be seen by the calculated chroma values. The closer the values are to 0, the more neutral the color is. The values shown here range from 1.68 to 11.05 and are relatively close to 0. While other scientists have demonstrated similar color neutrality, it is not a high priority for applications in greenhouses.

The main issues of the samples of this study are the lack of reproducibility, poor cycle stability, and low reversibility. Reasons for these issues are summarized in the following. First, the bubbles visible in Figure 1(b,c) are created during smart window production, as described in Section 5.1. The electrolyte shrinks during curing, which can cause air bubbles like those visible in Figure 1. These bubbles may contain oxygen. This leads to side reactions such as: $2CuCl + O_2 + Cl^{-} \longrightarrow 2CuO + Cl_2$ and $2Sn + O_2 \longrightarrow 2SnO$ [25]. It is assumed that these side reactions decrease the lifetime and reversibility of the device. Secondly, the hysteresis or aging effect of these samples has an impact. This means that previous measurements affect current ones. This is demonstrated by taking measurements with the same parameters and sample but getting different results. For example, Figure 5 shows the transmittance evolution during coloration at −1.5 V versus ITO for 60 s on the same sample. Although the same parameters and window were used, the green line shows faster coloration (40% per minute), compared to the blue line (11% per minute). Compared to Figure 3(a), the red line shows an even faster coloration of 55% per minute. The measurements in Figure 3(a) were taken after those shown in Figure 5. This leads to the assumption that the more the window switches, the faster and darker the coloration. This can be seen in Figure 3(a), where the lowest transmittance is 10%, while in Figure 5, the green line reaches about 25%. Another example is the different transmittance levels observed in different samples after coloration at −1.5 V versus ITO for 60 s. Window B (the green solid line in Figure 4(b)) shows a relatively small change in transmittance (77.5%–64.2%) compared to the data from Window A, which is probably due to the different histories of the two samples. While Window B had never been switched before, Window A had been used for several different tests (see Table 2). In [33], the hysteresis in RME devices is described as improved CE with an increased number of switching cycles. This aligns with our results. Hysteresis makes it difficult to compare measurements on the same

5928, 2026, 1, Downloaded from https://onlinelibrary.wiley.com/doi/10.1155/amse/9876638 by Dtsch Zentrum F. Luft-U. Raum Fahrt in D. Helmholtz Gemein., Wiley Online Library on [22/09/2026]. See the Terms and Conditions (https://onlinelibrary.wiley.com/terms-and-conditions) on Wiley Online Library for rules of use; OA articles are governed by the applicable Creative Commons License

sample and between samples, and is an issue that must be addressed before the window can be implemented in an application. Third, ITO degradation is a problem in RME smart windows [16] and is most likely the cause of the results shown in this study.

Nevertheless, the wide range of achievable transmittance observed here suggests a large adaptability of the windows to different application scenarios in principle.

4 | Conclusion

This study investigated a smart window with a solid-like electrolyte made of nontoxic components. The switching mechanism is based on RME using tin and copper. This novel electrolyte was demonstrated to have promising optical properties; however, it exhibited deficiencies in terms of cycle stability, reversibility, and reproducibility. An AVT ranging from 80.8% to 14.2% was achieved, and the device bleached with and without voltage application. The self-bleaching properties offer the potential for energy savings and design simplicity since only one direction of voltage application is needed to darken the smart window. Compared to Eh et al. [14], the smart window sample presented here exhibits higher transmittance in its initial state. Comprehensive investigations are necessary to systematically characterize the aging processes underlying the progressive decline in transmittance characteristics, alongside a thorough assessment of their integration into real-world usage scenarios. Further efforts are focused on the investigation of whether greenhouse systems equipped with smart windows can enhance crop yields. To achieve performance metrics comparable to contemporary RME-based smart window technologies, substantial improvements in cycle endurance and switching reversibility must be realized to ensure long-term device reliability and mitigate spectral fatigue over extended operational periods.

5 | Experimental Section

5.1 | Smart Window Production

The production of the smart window samples is separated into three steps: preparation of the glass with the ITO layer, production of the electrolyte, and assembly of the window. Samples A, B, C, and D were produced and are presented in this study. The production of the smart windows requires approximately three to 4 h, utilizing ITO-coated glass substrates. The ITO deposition process on the glass substrate is estimated to require an additional 3 h.

5.1.1 | Preparation of Glass with ITO

Schott D 263 T eco glass, which is 1.1 mm thick and 30×30 cm^2 in size, was used as the glass substrate. Prior to use, it was cleaned in a dishwasher with deionized water, as well as with acidic and alkaline cleaners. Then, the 30×30 cm^2 substrates were coated with a 60 nm ITO layer by sputtering in a Singulus Vistaris 600. This sample size leads to homogeneous deposition with reduced border effects. The glass was then cut into 5×5 cm^2 samples. A copper stripe was added to the ITO side of the glass to later connect the cables of the potentiostat. This can also be seen in the inset of Figure 1. A template was utilized to ensure that the copper stripes were placed in the same position relative to the electrolyte for each sample.

5.1.2 | Electrolyte Production

The foundation for the electrolyte's composition is derived from reference [32], with minor adjustments to ingredients and manufacturing processes. 964 mg of Type 1 Millipore filtered water was mixed with 112.8 mg of tin(II) chloride dihydrate ($SnCl_2 \cdot 2H_2O$) from Avantor with a purity of 98%. Subsequently, 85.2 mg of copper(II) chloride dihydrate ($CuCl_2 \cdot 2H_2O$) from Th. Geyer with a purity of 98% and 479 mg of lithium perchlorate ($LiClO_4$) from ThermoFisher with a purity greater than 99% were added. In another vessel, 9 g (90 wt%) of DMSO with a purity greater than 99% was heated to 120°C in an oil bath. Afterward, 0.94 g (8 wt%) of PVA with a purity of 99.3% was added in small portions to the DMSO while stirring with an electric stirrer. Once the mixture of DMSO and PVA was homogeneous, the temperature was reduced to 90°C. The stirrer was turned off while adding the metal mixture with a pipette to the DMSO solution. Some water evaporation likely occurred. Afterward, stirring should be started at a very slow speed to prevent the electrolyte from being pulled upward on the stirrer. Once the electrolyte was more dissolved, the speed was increased. While the mixture was stirred until homogeneous, the cold trap was filled with nitrogen for degassing. Stirring allows air to enter the electrolyte, which must be removed in the desiccator afterward. The pump was connected to the cold trap and the desiccator. After stirring the mixture, it was placed in the desiccator for at least 30 min. Then, the electrolyte was ready for window assembly. A picture of the cured electrolyte can be found in Figure S1 of the supporting information.

5.1.3 | Window Assembly

A 0.5 mm thick polytetrafluoroethylene (PTFE) sealing ring was glued to the indium-tin oxide (ITO)-coated side of a 5×5 cm^2 glass substrate. A template was employed to standardize the positioning of the copper stripes among the samples. The liquid electrolyte, which had not yet solidified, was then introduced into the sealing ring until it occupied the entire available space. Subsequently, a second ITO-coated glass substrate was placed on top of the sealing ring with the ITO facing the electrolyte. The sealing ring was glued to the second substrate under pressure. The resulting window sample was cured overnight and stabilized with Kapton tape. See the inlays of Figure 1(b,c).

5.2 | Measurement Devices

5.2.1 | UV–Vis–NIR Spectrometer

A Cary 5000 spectrophotometer from Agilent was used for all transmittance measurements, which included a zero/baseline correction. Transmittance measurements were taken between 200 and 2500 nm, with a scan rate of 400 nm per minute and a step size of 5 nm. For time-resolved measurements, such as those shown in Figures 2 and 4, the transmittance was measured between 540 and 560 nm at a rate of 200 nm per minute with a step length of 5 nm, and the values were averaged.

5.2.2 | Potentiostat

A Versastat 4 from Ametek was used to conduct electrochemical measurements. In this study, the cyclic voltammetry, open circuit

5928, 2026, 1, Downloaded from https://onlinelibrary.wiley.com/doi/10.1155/amse/9976638 by Dtsch Zentrum F. Luft-U. Raum Fahrt in D. Helmholtz Gemein., Wiley Online Library on [22/09/2026]. See the Terms and Conditions (https://onlinelibrary.wiley.com/terms-and-conditions) on Wiley Online Library for rules of use; OA articles are governed by the applicable Creative Commons License

voltage, and constant voltage modes were used to change and measure the electrical properties of smart windows. The exact values used for voltage application are mentioned before and shown in Table 2. It should be noted that the applied potentials are always measured against the ITO electrode, not a separate reference electrode.

5.2.3 | Combined Measurement

For the combined measurement, the sample was placed in the UV–Vis–NIR spectrometer and connected to the potentiostat. The first transmittance measurement was taken before any voltage was applied, in order to observe the initial state of the window sample. Subsequent transmittance measurements were taken during voltage application at predetermined time intervals, which were dependent on the total measurement duration and the duration of a single measurement [25].

Acknowledgments

The authors thank Nico Ruskaup for producing the ITO layers with the Singulus Vistaris 600 sputter machine. The authors also thank Alexander Gräfenstein for support during the preparation and production of the electrolyte and Anna Ullrich of TU Chemnitz for proofreading the manuscript. The authors are further grateful to Guo et al. for sharing their data.

Funding

This work was performed while employed at the Deutsches Zentrum für Luft- und Raumfahrt. Open access funding enabled and organized by Projekt DEAL.

Conflicts of Interest

The authors declare no conflicts of interest.

Data Availability Statement

The data supporting the findings of this study are available from the corresponding author upon reasonable request.

References

1. United Nations Environment Programme, *Buildings and Climate Change: Summary for Decision Makers* (2009), https://wedocs.unep.org/20.500.11822/32152.

2. E. S. Lee, M. Yazdanian, and S. E. Selkowitz, *The Energy-Savings Potential of Electrochromic Windows in the US Commercial Buildings Sector* (Berkeley Lab, 2004), https://buildings.lbl.gov/publications/energy-savings-potential.

3. N. L. Sbar, L. Podbelski, H. M. Yang, and B. Pease, "Electrochromic Dynamic Windows for Office Buildings," *International Journal of Sustainable Built Environment* 1, no. 1 (2012): 125–139, https://doi.org/10.1016/j.ijsbe.2012.09.001.

4. A. Hedge and C. McKee, "Employee Reactions to Electrochromic Glass Windows in a Financial Office Building," *Proceedings of the Human Factors and Ergonomics Society-Annual Meeting* 64, no. 1 (2020): 531–535, https://doi.org/10.1177/1071181320641120.

5. M. Brzezicki, "A Systematic Review of the Most Recent Concepts in Smart Windows Technologies With a Focus on Electrochromics: Review," *Sustainability* 13.17 (2021): 9604, https://doi.org/10.3390/su13179604.

6. H. Sarmadi and M. Mahdavinejad, "A Designerly Approach to Algae-Based Large Open Office Curtain Wall Facades to Integrated Visual Comfort and Daylight Efficiency," *Solar Energy* 251 (2023): 350–365, https://doi.org/10.1016/j.solener.2023.01.021.

7. M. N. Mustafa, M. A. A. Mohd Abdah, A. Numan, A. Moreno-Rangel, A. Radwan, and M. Khalid, "Smart Window Technology and Its Potential for Net-Zero Buildings: A Review," *Renewable and Sustainable Energy Reviews* 181 (2023): 113355, https://doi.org/10.1016/j.rser.2023.113355.

8. Z. Wen, Y. Ke, C. Feng, et al., "Mg–Doped VO_2 @ZrO_2 Core−Shell Nanoflakes for Thermochromic Smart Windows With Enhanced Performance," *Advanced Materials Interfaces* 8, no. 1 (2021): 2196–7350, https://doi.org/10.1002/admi.202001606.

9. Grand View Research Inc, *Global Smart Glass Market Size & Outlook* (2024), 2024–2030, https://www.grandviewresearch.com/industry-analysis/smart-glass-market.

10. C. W. Moon, N. C. Bhoumik, P. Mondol, S. H. Park, H. W. Jang, and C. J. Barile, "Origin of High Optical Contrast in Zinc-Zinc Oxide Electrodeposits for Dynamic Windows," *Nano Energy* 114 (2023): 108666, https://doi.org/10.1016/j.nanoen.2023.108666.

11. M. Son, D. Shin, and C. S. Lee, "Facile Fabrication of Trimodal Switchable Mirror Device With Zero Transmittance in the Black State," *Advanced Materials Interfaces* 8, no. 3 (2021): 2196–7350, https://doi.org/10.1002/admi.202001416.

12. G. P. T. Ganesh and B. Deb, "Designing an All–Solid–State Tungsten Oxide Based Electrochromic Switch With a Superior Cycling Efficiency," *Advanced Materials Interfaces* 4, no. 14 (2017): 2196–7350, https://doi.org/10.1002/admi.201700124.

13. C. Bechinger, J. N. Bullock, J. G. Zhang, et al., "Low-Voltage Electrochromic Device for Photovoltaic-Powered Smart Windows," *Journal of Applied Physics* 80, no. 2 (1996): 1226–1232, https://doi.org/10.1063/1.363731.

14. A. L. S. Eh, *Reversible Electrochemical Mirror Devices* (2020), https://doi.org/10.32657/10356/146626.

15. C. J. Barile, D. J. Slotcavage, J. Hou, M. T. Strand, T. S. Hernandez, and M. D. McGehee, "Dynamic Windows With Neutral Color, High Contrast, and Excellent Durability Using Reversible Metal Electrodeposition," *Joule* 1, no. 1 (2017): 133–145, https://doi.org/10.1016/j.joule.

16. T. S. Hernandez, M. Alshurafa, M. T. Strand, et al., "Electrolyte for Improved Durability of Dynamic Windows Based on Reversible Metal Electrodeposition," *Joule* 4, no. 7 (2020): 1501–1513, https://doi.org/10.1016/j.joule.2020.05.008.

17. M. T. Strand, C. J. Barile, T. S. Hernandez, et al., "Factors That Determine the Length Scale for Uniform Tinting in Dynamic Windows Based on Reversible Metal Electrodeposition," *ACS Energy Letters* 3, no. 11 (2018): 2823–2828, https://doi.org/10.1021/acsenergylett.8b01781.

18. C. Sui, J. Pu, T. H. Chen, et al., "Dynamic Electrochromism for All-Season Radiative Thermoregulation," *Nature Sustainability* 6, no. 4 (2023): 428–437, https://doi.org/10.1038/s41893-022-01023-2.

19. X. Tao, D. Liu, J. Yu, and H. Cheng, "Reversible Metal Electrodeposition Devices: An Emerging Approach to Effective Light Modulation and Thermal Management," *Advanced Optical Materials* 9, no. 8 (2021): 2195–1071, https://doi.org/10.1002/adom.202001847.

20. S. M. Islam and C. J. Barile, "Dynamic Windows Using Reversible Zinc Electrodeposition in Neutral Electrolytes With High Opacity and Excellent Resting Stability," *Advanced Energy Materials* 11, no. 22 (2021): 1614–6832, https://doi.org/10.1002/aenm.202100417.

21. B. M. Howard and J. P. Ziegler, "Optical Properties of Reversible Electrodeposition Electrochromic Materials," *Solar Energy Materials and Solar Cells* 39, no. 2–4 (1995): 309–316, https://doi.org/10.1016/0927-0248(95)00065-8.

22. Y. Zhang, B. Xu, B. Huang, et al., "Color-Neutral Smart Window Enabled by Gradient Reversible Alloy Deposition," *ACS Energy Letters* 9, no. 8 (2024): 4162–4171, https://doi.org/10.1021/acsenergylett.4c01677.

5928, 2026, 1, Downloaded from https://onlinelibrary.wiley.com/doi/10.1155/amse/9976638 by Dtsch Zentrum F. Luft-U. Raum Fahrt in D. Helmholtz Gemein., Wiley Online Library on [22/09/2026]. See the Terms and Conditions (https://onlinelibrary.wiley.com/terms-and-conditions) on Wiley Online Library for rules of use; OA articles are governed by the applicable Creative Commons License

23. F. Zhao, B. Wang, B. Huang, et al., "Inorganic Electrochromic Smart Windows for Advancing Building Energy Efficiency," *Nature Reviews Clean Technology* 1.6, no. 6 (2025): 396–412, https://doi.org/10.1038/s44359-025-00065-x.

24. Y. Cai, Z. Li, T. S. Hernandez, et al., "Dynamic Windows Based on Reversible Silver Electrodeposition With Improved Resting Stability and Cyclability," *Cell Reports Physical Science* 6, no. 5 (2025): 102559, https://doi.org/10.1016/j.xcrp.2025.102559.

25. A. L. S. Eh, "A Quasi-Solid-State Tristate Reversible Electrochemical Mirror Device With Enhanced Stability," *Advanced Science* 7, no. 13 (2020): 1903198, https://doi.org/10.1002/advs.201903198.

26. R. J. Mortimer, D. R. Rosseinsky, and P. M. S. Monk, eds., in *Electrochromic Materials and Devices* (Wiley-VCH Verlag GmbH & Co KGaA, 2015).

27. Y. Alesanco, J. Palenzuela, A. Viñuales, G. Cabañero, H. J. Grande, and I. Odriozola, "Polyvinyl Alcohol-Borax Slime as Promising Polyelectrolyte for High-Performance, Easy-to-Make Electrochromic Devices," *ChemElectroChem* 2, no. 2 (2015): 218–223, https://doi.org/10.1002/celc.201402265.

28. P. Cossari, M. Pugliese, C. Simari, et al., "Simplified All-Solid-State WO_3 Based Electrochromic Devices on Single Substrate: Toward Large Area, Low Voltage, High Contrast, and Fast Switching Dynamics," *Advanced Materials Interfaces* 7, no. 3 (2020): 2196–7350, https://doi.org/10.1002/admi.201901663.

29. S. C. de Oliveira, L. C. de Morais, A. A. da Silva Curvelo, and R. M. Torresi, "An Organic Aqueous Gel as Electrolyte for Application in Electrochromic Devices Based in Bismuth Electrodeposition," *Journal of the Electrochemical Society* 150, no. 11 (2003): E578, https://doi.org/10.1149/1.1615610.

30. J. X. Hou, W. Zhou, S. Zhang, S. Hou, and M. Sheng, "Investigation of Structure and Properties of Rapidly Solidified CuSn Alloy," *International Journal of Electrochemical Science* 10.10, no. 10 (2015): 8558–8568, https://doi.org/10.1016/S1452-3981(23)11119-9.

31. S. Ahrland, et al., "The Stability of Metal Halide Complexes in Aqueous Solution. VII. The Chloride Complexes of Copper(I)," *Acta Chemica Scandinavica* 24 (1970): 157–172, https://doi.org/10.3891/acta.chem.scand.24-0157.

32. X.-Y. Yu, "Fabrication and Characterization of PEO/PPC Polymer Electrolyte for Lithium-Ion Battery," *Journal of Applied Polymer Science* 115, no. 5 (2010): 2718–2722, https://doi.org/10.1002/app.29915.

33. T. S. Hernandez, C. J. Barile, M. T. Strand, T. E. Dayrit, D. J. Slotcavage, and M. D. McGehee, "Bistable Black Electrochromic Windows Based on the Reversible Metal Electrodeposition of Bi and Cu," *ACS Energy Letters* 3, no. 1 (2018): 104–111, https://doi.org/10.1021/acsenergylett.7b01072.

34. W. Kao-ian, M. Nguyen, T. Yonezawa, et al., "Highly Stable Rechargeable Zinc-Ion Battery Using Dimethyl Sulfoxide Electrolyte," *Materials Today Energy* 21 (2021): 100738, https://doi.org/10.1016/j.mtener.2021.100738.

35. D. Aurbach, *Nonaqueous Electrochemistry* (CRC Press, 1999), https://doi.org/10.1201/9780367800499.

36. X. Guo, S. Chen, W. C. Poh, et al., "Solid-State and Flexible Black Electrochromic Devices Enabled by Ni-Cu Salts Based Organohydrogel Electrolytes," *Advanced Materials Interfaces* 10, no. 15 (2023): 2196–7350, https://doi.org/10.1002/admi.202300061.

37. *Colorimetry-Part 4: CIE 1976 L*A*B Colour Space*, 6 (2019).

38. X. Guo, J. Chen, A. L. S. Eh, et al., "Heat-Insulating Black Electrochromic Device Enabled by Reversible Nickel-Copper Electrodeposition," *ACS Applied Materials and Interfaces* 14, no. 17 (2022): 20237–20246, https://doi.org/10.1021/acsami.2c02626.

39. M. T. Strand, T. S. Hernandez, M. G. Danner, et al., "Polymer Inhibitors Enable > 900 cm^2 Dynamic Windows Based on Reversible Metal Electrodeposition With High Solar Modulation," *Nature Energy* 6, no. 5 (2021): 546–554, https://doi.org/10.1038/s41560021-00816-7.

Supporting Information

Additional supporting information can be found online in the Supporting Information section.

Supporting Information is available from the Wiley Online Library or from the authors. **Supporting Information 1.** Video 1 shows the coloration of Window A. For the coloration, −1.5 V versus ITO was applied for 60 s. **Supporting Information 2.** Video 2 shows the bleaching of Window A. For the bleaching, 0.3 V versus ITO was applied for 60 s. **Supporting Information 3.** Figure S1: Cured electrolyte in a bottle.

5928, 2026, 1, Downloaded from https://onlinelibrary.wiley.com/doi/10.1155/amse/9976638 by Dtsch Zentrum F. Luft-U. Raum Fahrt in D. Helmholtz Gemein., Wiley Online Library on [22/09/2026]. See the Terms and Conditions (https://onlinelibrary.wiley.com/terms-and-conditions) on Wiley Online Library for rules of use; OA articles are governed by the applicable Creative Commons License